Effect of tethering chemistry of cationic surfactants on clay exfoliation, electrospinning and diameter of PMMA/clay nanocomposite fibers

Citation: Wang, M., J.H. Yu, A.J. Hsieh, and G.C. Rutledge. "Effect of Tethering Chemistry of Cationic Surfactants on Clay Exfoliation, Electrospinning and Diameter of PMMA/clay Nanocomposite Fibers." Polymer 51, no. 26 (December 2010): 6295–6302.

As Published: http://dx.doi.org/10.1016/j.polymer.2010.10.040

Publisher: Elsevier

Persistent URL: http://hdl.handle.net/1721.1/101240

Version: Author's final manuscript: final author's manuscript post peer review, without publisher's formatting or copy editing

Effect of tethering chemistry of cationic surfactants on clay exfoliation, electrospinning and diameter of PMMA/clay nanocomposite fibers

M. Wang[a], J. H.Yu[a*], A. J.Hsieh[b], G.C. Rutledge[a]

[a]Department of Chemical Engineering and Institute for Soldier Nanotechnologies, Massachusetts Institute of Technology, Cambridge, MA 02139

[b]Army Research Laboratory, RDRL-WMM-G, Aberdeen Proving Ground, MD 21005-5069, USA

*Current address: Army Research Laboratory, RDRL-WMM-B, Aberdeen Proving Ground, MD 21005-5069, USA

Abstract:

We examine the influence of tethering chemistry of cationic surfactants on exfoliation of montmorillonite (MMT) clay dispersed in methyl methacrylate (MMA) followed by in-situ polymerization to form polymethyl methacrylate (PMMA), the effect of exfoliation and clay loading on the rheology of polymer/clay dispersions in dimethyl formamide, and the diameters of nanocomposite fibers formed from these dispersions by electrospinning. Incorporation of an additional reactive tethering group of methacryl functionality significantly improves the intercalation and exfoliation of clays in both in-situ polymerized PMMA nanocomposites and the corresponding electrospun fibers. The proper surfactant chemistry also increases the dispersion stability, extensional viscosity, extent of strain hardening and thus the electrospinnablity of the nanocomposite dispersions, especially at low nanocomposite concentrations. The degree of the enhancement in electrospinnability by clays with proper tethering chemistry is at least the same as or greater than that obtained with three times higher loading level of clay

particles without proper tethering chemistry in the nanocomposites. The diameters of electrospun nanocomposite fibers are mostly determined by the solids content, which consists primarily of polymer components. The effect of small amounts of clay particles in the nanocomposite dispersions on the diameter of electrospun fibers is minimal. These results suggest a new strategy to produce smaller diameter fibers from very dilute polymer solutions, which are otherwise not electrospinnable, by incorporating a small amount of well-exfoliated clays.

Introduction:

Electrospinning is an effective method for producing polymer fibers with diameters ranging from tens of nanometers to microns [1-2]. Due to the small diameters of the fibers, there has been significant interest in this technique for a wide variety of potential applications [3-11]. In general, the diameter of the electrospun fibers decreases with the polymer concentration in solution. However, "electrospinnability", the ease with which uniform fibers are formed from the polymer solution by electrospinning, is also compromised by the decrease in the polymer concentration in solution. When the polymer concentration is too low, polymer drops or the beads-on-string morphology is obtained instead of continuous, uniform fibers. Therefore it is desirable to develop strategies to increase the electrospinnability of polymer solutions, especially at low concentrations, in order to produce smaller diameter fibers. This is particularly important for applications such as transparent nanocomposites, filter media and non-wetting materials, where small fibers are highly desirable.

Several strategies have been devised to improve the ability of spinning fibers from solutions at low concentration. One of these employs a coaxial electrospinning technology to process the otherwise non-fiber-forming solution as the core fluid within a shell of a second fluid that readily forms fibers [12]. The elasticity of the shell fluid serves to stabilize the coaxial jet, resulting in solid fibers with core-shell morphology; the shell may subsequently be removed to yield small diameter fibers comprised of the core component. A second approach involves blending a small quantity of a miscible, high molecular weight polymer to the spin dope [13-14]. The result is fiber of blended composition. The effectiveness of this approach can be rationalized in terms of an increase in the elasticity of the solution [15], which in turn can often be traced to an increase in entanglement density [16-18] or similar associative effects [19]. On the other hand, adding nanoparticles such as clay particles into polymer solutions have been shown to be very effective in increasing both shear viscosity and extensional viscosity of polymer/nanoparticle dispersions, which are mainly due to the interactions between the polymers and the nanoparticles and between the nanoparticles [20-22]. Thus, electrospinning polymer/nanoparticle dispersions could be another effective strategy to form fibers from solutions at low concentrations.

Clay particles have been shown to be easily electrospun with different polymers such as nylon 66, poly(vinyl alcohol), poly(vinylidene fluoride) for various applications [23-28]. In a previous paper, we demonstrated success in electrospinning of poly(methyl methacrylate) (PMMA) -based nanocomposites into fibers of submicron diameter [29]. Addition of clays into polymer solutions increased the extensional viscosity, the extent of strain hardening and thus the electrospinnability of the resulting polymer/clay dispersions.

The electrospun PMMA nanocomposite fibers showed enhanced thermal stabilities at high temperatures over the electrospun pristine polymeric fibers. Nanocomposite fibers electrospun from other polymer/clay dispersions were also shown to exhibit enhanced mechanical properties, such as shear modulus, and higher thermal properties, such as glass transition temperature [30-34]. Electrospun fibers could be further used as the reinforcing agents in polymer-based composites to improve the physical and mechanical properties of composites [35]. Electrospinning of PEO/laponite solution indicated a universal correlation between fiber diameter and solution properties that does not include shear viscosity as a primary variable [36]. However, the enhancement of electrospinnability and fiber properties depends largely on the exfoliation of the clays and/or their loading levels in the dispersion.

Layered silicates, also known as clays, are hydrophilic in nature. To improve their compatibility with hydrophobic polymers, the silicate surfaces are usually modified with alkyl ammonium cationic surfactants through an ion exchange reaction. The cationic head groups of the alkyl ammonium molecules preferentially reside at the surface of the negatively charged layered silicate, while the oligomeric hydrocarbon species extend into the galleries and render the original hydrophilic silicate surface to be organophilic[37-40]. Polymer nanocomposites may be prepared by melt blending, in-situ polymerization or solution blending. The advantage of in-situ polymerization is the potential to yield a nanocomposite with very high degree of dispersion and exfoliation of layered silicates without the need for high shear forces required in melting processing [41-44]. During in-situ polymerization, the monomers first diffuse into the galleries of chemically modified

layered silicates, then polymerize, resulting in expansion of the gallery spacing that leads to exfoliated structure [45-48]. Therefore, it is very important to ensure the chemical affinity between the monomer and the surfactant in order to facilitate the monomer diffusion into the gallery to achieve better exfoliation. From the thermodynamic point of view, a favorable interaction between the surfactant and polymer matrix helps to maintain the stability of exfoliated morphology and to resist platelet re-aggregation during the post-processing of polymer nanocomposites, such as thermal pressing or dissolution in solvent [49-50].

The objective of this paper is to determine the proper tethering chemistry of surfactants to increase the exfoliation of the clays, which then further increases the electrospinnability of in-situ polymerized PMMA/clay dispersions, especially at low concentrations of polymer and clay in the dispersion. The effect on electrospinning by proper tethering chemistry of surfactants is compared to that obtained by increasing the loading levels of clay particles in the nanocomposites. The effect of adding organically modified clay particles on the diameter of the electrospun fibers is also studied.

Experimental:

Synthesis of polymer nanocomposites:

Two types of synthetic alkyl ammonium surfactants with an additional tethering group of either methacryl or styryl functionality prepared by Triton Systems, Inc. (Chelmsford, M.A.) were used. Their chemical structures are shown in Figure 1. A commercial clay, (Cloisite™ 20A, Southern Clay Products, Inc., Gonzales, Texas) consisting of dehydrogenated dimethyl tallow quaternary ammonium surfactant was also

used for comparison. The sample designation, surfactant chemistry, cation exchange capacity (CEC) and inter-gallery spacing ([001] d-spacing, as measured by wide angle x-ray diffraction) of the organically modified clays used in this work are listed in Table 1.

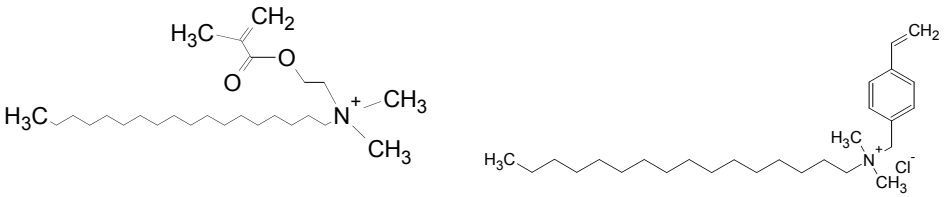

(a) (b)

Figure 1: Alkyl ammonium surfactants with tethering group of either (a) methacryl or (b) styryl functionality.

PMMA nanocomposites were prepared by Triton Systems, Inc. via in-situ polymerization. In general, a specified amount of organically modified clay was added into the methyl methacrylate (MMA) monomer, followed by thorough mixing via sonication under nitrogen to promote intercalation. An equal weight of PMMA prepolymer (Mw=55 kg/mol) were added into the above clay/MMA mixture, followed by benzoyl peroxide initiator (0.75% wt./wt . MMA). The mixture was then stirred vigorously for 10 mins before it was cast and stored at 50ºC for at least 12 hours. The cast samples were then annealed at 100°C for one hour before any testing.

The materials used in this study are designated as follows: A, B and C are organically modified clays, in which A has a methacryl-tethering group, B has a styryl-tethering group, and C is commercial Cloisite™ 20A; NA, NB and NC are the in-situ

polymerized nanocomposites prepared from the corresponding clays A, B and C. Both NA and NB have a 2.5 wt% loading of the corresponding organically modified clays, while NC1, NC2 and NC3 have 2.5, 5 and 7.5 wt.% loading of clay C, respectively.

Table 1: Specifications of organically modified MMT clays:

Designation of organically modified clays	Surfactant chemistry	CEC (meq/100g clay)	Basal spacing (nm)
A	Methacryl-tethering	93	1.975
B	Styryl-tethering	93	2.079
C	Cloisite™ 20A	95	2.42

Electrospinning: PMMA solutions or PMMA/clay dispersions were prepared by dispersing the polymer or nanocomposite (i.e. polymer plus clay) at concentrations of 6 and 10 wt.% in dimethyl formamide (DMF). The solutions and dispersions were vigorously stirred for at least 72 hours at room temperature. A parallel-disk electrospinning apparatus was used in this study, as described by Shin et al. and Fridrikh et al. [51-52]. The electric field, solution flow rate and distance between the two parallel plates were adjusted to obtain a stable jet.

Characterization: Transmission electron microscopy (TEM) was performed on a JEOL JEM200 CX TEM microscope (JEOL Ltd, Japan). Wide-angle X-ray diffraction (WAXD) data were obtained using a diffractometer (Bruker, Madison,WI) with CuKα radiation at 40 kV and 20 mA. Images of fibers were taken using a JEOL-6060 scanning electron microscope (SEM) (JEOL Ltd, Japan). Molecular weight analysis was

performed by gel permeation chromatography (GPC) with a PLgel mixed-C Column (300 x 7.5 mm and pore size 5μm) (Polymer Laboratories, Inc., UK) and a Waters 2414 refractive index detector. All measurements were carried out at a flow rate of 1 mL/min at 35 °C with tetrahydrofuran (THF) as the carrier solvent. Polystyrene standards were used for calibration. For GPC measurements, nanocomposite dispersions of 0.5 wt.% in THF were centrifuged using a Centrifuge 5804R (Eppendorf AG, Germany) at 5000 rpm for 15 min. The supernatent was taken out by a syringe and filtered using 0.1 μm Puradisk^{TM} PTFE filter (Whatman plc,UK) for GPC measurements.

Shear rheology was performed using an AR2000 Rheometer (TA Instruments, New Castle, DL) at 25ºC using a parallel disk geometry with 40 mm diameter plates. Steady shear measurements were carried out at constant shear rates ranging from 1 to 1000 s^{-1}. Low amplitude oscillatory shear measurements were performed by applying a time dependent strain $\gamma(t) = \gamma_0 \sin(\omega t)$, where ω is the frequency and t is the time. The resulting time dependent shear stress is $\tau(t)=\gamma_0[G'\sin(\omega t)+G''\cos(\omega t)]$ where G' is the storage modulus, and G'' is the loss modulus. The linear viscoelastic moduli reported here were confirmed to be independent of the strain amplitude by repeating measurements at two different strain amplitudes of 1% and 2 %. Extensional rheological measurements were performed on a HAAKE CaBER 1 rheometer (Thermo Electron Corporation,WI).

Results and Discussion:

Characterization of PMMA nanocomposites:

***Morphology analysis*:**

Figure 2 compares the effect of different surfactant chemistries on WAXD spectra of in-situ polymerized PMMA nanocomposites that have the same clay loading level, 2.5 wt.%. NC1 displays a broad peak at about 2θ=2.50º with a corresponding d-spacing of 3.4 nm. NB shows a very broad peak around 2θ= 3.4º (d=2.5 nm) and perhaps a small shoulder at 2θ=2.37º (d=3.7 nm), which we attribute to a second order basal plane reflection and a shoulder on the primary reflection, respectively. NA is almost featureless in WAXD, indicating best dispersion among the three organically modified clays, due either to exfoliation, extensive intercalation resulting in shift of the basal plane reflection below the limit of detection in 2θ, or both. Figure 3 compares TEM images of the corresponding PMMA nanocomposites. Both NA and NB show smaller average tactoid size, but higher number of tactoids per unit area than NC1. NA has slightly smaller average tactoid size and slightly higher number of tactoids per unit area than NB. These results indicate that the size of clay particles was greatly reduced and clay particles were best dispersed in NA, then NB, and NC the least [50]. The difference in the morphologies of these PMMA nanocomposites is mainly attributed to the difference in compatibility between the pretreated surfactants and the MMA monomer during in-situ polymerization. Clay A possesses surfactant with methacryl-tethering group similar to the chemical structure of MMA, whereas B has surfactant with styryl tethering group and C has no tethering functionality. The presence of the methyacryl-tethering group presumably facilitates the diffusion of MMA monomers into the galleries of clay and promotes the intercalation and exfoliation of clays in PMMA matrix throughout the in-situ polymerization. In addition, reaction of the unsaturated vinyl groups in both clays A and B with the MMA monomer during in-situ polymerization further improves the

exfoliation of clays [53-54]. WAXD spectra and TEM images of NC2 and NC3 (not shown) displayed similar patterns as those of NC1, except increased peak intensities in WAXD and higher concentrations of clay tactoids in TEM images.

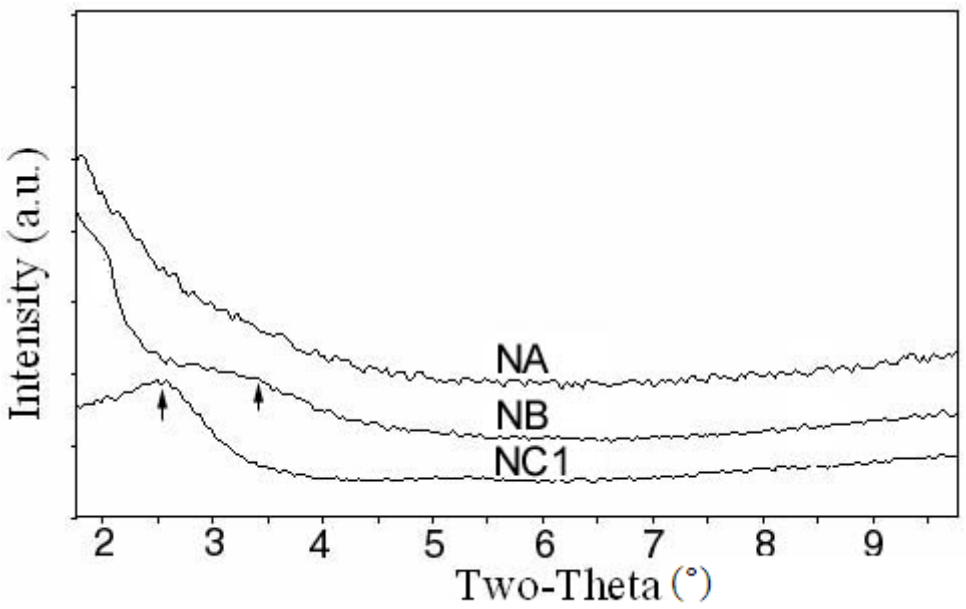

Figure 2: Comparison of WAXD spectra of three in-situ polymerized PMMA nanocomposites at the same clay loading level of 2.5 wt%: NA, NB and NC1.

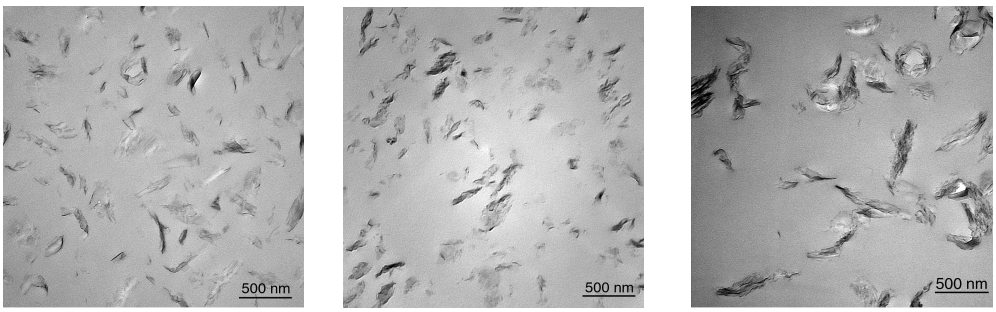

(a) (b) (c)

Figure 3: Comparison of TEM images of in-situ polymerized PMMA nanocomposites at the same clay loading level of 2.5wt%, (a) NA, (b) NB, (c) NC1.

Rheology:

Immediately after preparation, all PMMA/clay dispersions in DMF solvent were homogeneous and translucent. After storing at room temperature for two weeks, the dispersion of NC1 settled down to the bottom and phase separation occurred, while the NA and NB dispersions remained homogeneous, as shown in Figure 4. This indicates that reactive tethering groups in A and B help to preserve the intercalated and/or exfoliated microstructure and prevent the re-aggregation of clay tactoids or platelets in DMF. This improvement in dispersion stability for extended period is very important, particularly for solvent-based processing such as electrospinning.

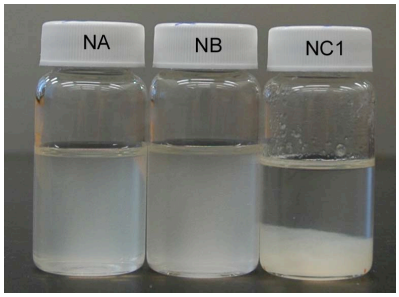

Figure 4: The appearance of 6 wt% PMMA nanocomposite dispersions in DMF after storage for two weeks.

From GPC measurements, similar Mw averages and distributions (not shown) were obtained for the pure PMMA and for the PMMA matrix component of the

nanocomposites obtained after centrifugation. These data indicate that the difference in the rheology of pure PMMA solution and the PMMA/clay dispersions does not arise from the variation in the molecular weights of the PMMA matrix.

***Steady Shear rheology*:**

The shear viscosity as a function of shear rates for 10 wt.% PMMA solution and 10 wt% PMMA/clay dispersions measured at room temperature are compared in Figure 5. The pure PMMA solution behaves like a typical shear thinning fluid, with a plateau in viscosity at low shear rates. For NC1, NC2 and NC3, the viscosity increased monotonically with the clay loading from 2.5 to 7.5 wt.%. As seen in Figure 5, even at low shear rates <1 s^{-1}, pronounced shear thinning is observed in the NC2 and NC3 dispersions, while the NC1 dispersion exhibits predominantly a plateau in viscosity, as does the PMMA solution, but with a lower onset shear rate for shear thinning. This is due to the higher concentration of clays in the NC2 and NC3 dispersions, which facilitated the ordering of clay particles in the flow direction and induced the shear thinning behavior at low shear rates [55-57]. For nanocomposites having the same clay loading (2.5 wt.%) but different surfactants, the NA dispersion shows higher viscosity than the NB dispersion, and both have higher viscosities than the NC1 dispersion. This difference in viscosity, especially at low shear rates, was mainly attributed to better intercalation and/or exfoliation of clay particles in NA, then NB, and the least NC1, as shown from the results of X-ray and TEM analyses. At low shear rates, the NA dispersion shows even higher shear viscosity than the NC2 dispersion, and the latter has almost twice the clay loading of the former. At high shear rates (>1000 s^{-1}, Figure 5),

shear viscosity for PMMA solution and all polymer/clay dispersions are comparable, indicative of the preferential alignment and orientation of clay particles in the flow direction [57].

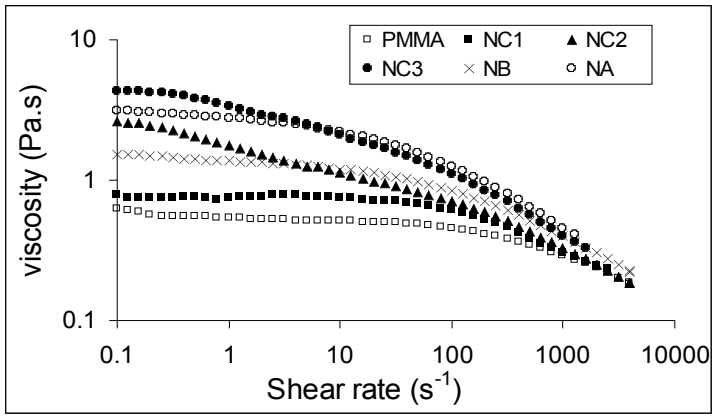

Figure 5. Steady shear viscosity as a function of shear rate measured at room temperature for 10 wt.% PMMA solution and 10 wt.% PMMA/clay dispersions.

***Dynamic Shear Rheology*:**

The effects of clay loading and surfactant chemistry on the dynamic shear rheology of the 10 wt.% PMMA/clay dispersions are compared in Figure 6. For the NC dispersions both storage modulus, G', and shear modulus, G", increased monotonically with clay loading at all frequencies. For the dispersions having the same clay loading, but different surfactant chemistry, the NA dispersion exhibits the highest G' and G" values, followed by the NB dispersion and then the NC1 dispersion. This indicates that clay particles exhibit the best intercalation and/or exfoliation in NA, followed by NB and then

by NC1. These results are consistent with the observations in WAXD, TEM and steady shear rheology. The G' and G" values for the NA dispersion are comparable with those for the NC2 dispersion, yet the latter has almost double the amount of clay loading compared to the former.

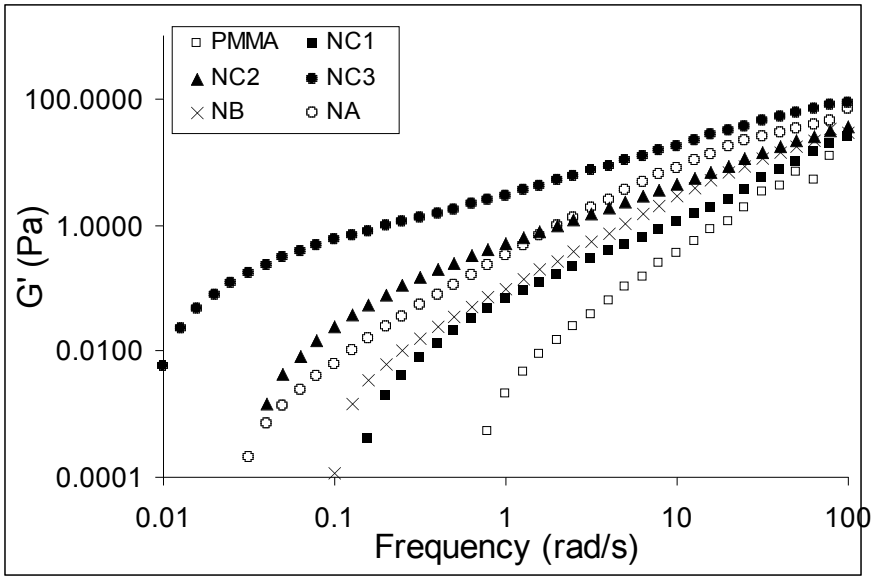

(a)

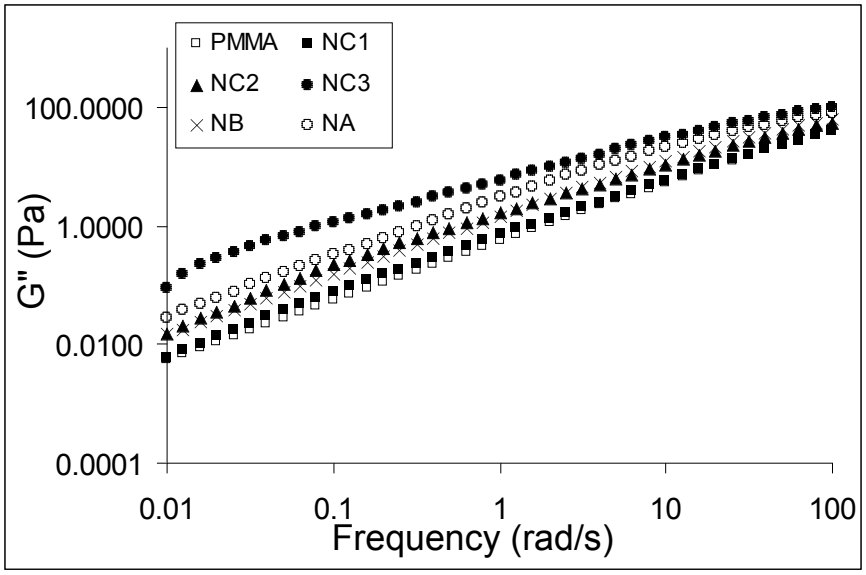

(b)

Figure 6. Dynamic shear rheology data as a function of frequency for the 10 wt.% PMMA solution and 10 wt.% PMMA/clay dispersions: (a) storage modulus, G', and (b) loss modulus, G".

Extensional Rheology:

Extensional rheology of PMMA solution and polymer/clay dispersions were measured using a capillary breakup extensional rheometer (CaBER). The time evolution of the midpoint diameter of the fluid filament of the 10 wt.% PMMA solution and polymer/clay dispersions in DMF are shown in Figure 7a. The PMMA solution has the fastest rate of capillary thinning, and incorporation of clay apparently decreases the rate of capillary thinning for the polymer/clay dispersions. For the NC dispersions, the rate of capillary thinning decreases as the clay loading increases. Among nanocomposites having

the same clay loading level but different surfactants, the NA dispersion shows the slowest rate of capillary thinning, followed by the NB dispersion, and then the NC1 dispersion. The values of apparent extensional viscosity versus Hencky strain, calculated from the capillary thinning data by following the approach described in a previous paper [51], are shown in Figure 7b. The extensional viscosity at low Hencky strain as well as the extent of strain hardening increased with the clay loading for the NC dispersions. Among the nanocomposite dispersions having the same clay loading but different surfactant chemistry, the NA dispersion shows the highest extensional viscosity as well as extent of strain hardening, followed by the NB dispersion, and then the NC1 dispersion, similar to the shear viscosities. However, the magnitude of increment in the extensional viscosity of NA or NB dispersions resulting from proper surfactant chemistry is far more significant than that in the shear viscosity. The NA dispersion exhibits higher extensional viscosity than the NC3 dispersion, contrary to the observations in shear rheology. Likewise, higher extensional viscosity but lower shear viscosity was observed in the NB dispersion, compared to that in NC2. These results indicate that the influence of proper surfactant chemistry is more significant in the increase of extensional viscosity than in the shear viscosity of polymer/clay dispersions.

The characteristic time for filament thinning, λ_c, correlates with the longest (Zimm) relaxation time of the fluid. It characterizes the natural time scale for the fluid's response to stress, such as that due to capillary forces in the CaBER experiment. These relaxation times were measured for both the polymer solution and the polymer/clay dispersions from curve fitting of the extensional rheology data by an elastic model, as described in a previous paper [50]. The longest relaxation times are then used to compute

a Deborah number, De, that characterizes the natural response time of the fluid relative to the relevant time scale for the process, in this case the breakup of the jet into droplets. For the latter, we use the method described by Chen et al [58] to compute the Rayleigh instability growth rate, assuming a jet of pure DMF and the inner spinneret diameter of R_0=0.8 mm. We then take the inverse of the growth rate as the process time scale. If De >>1, indicating the relaxation time is much greater than instability growth time, the instability is fully suppressed or arrested by the viscoelastic response to produce uniform fibers. Table 2 shows the values of the relaxation times, λ_c, the filament break up time t_b, and the De value obtained for the PMMA solution and each of the PMMA/clay dispersions. All the λ_c , t_b and De values increase monotonically with clay loading for the NC dispersions, presumably due to filler-filler and polymer-filler interactions [51,59-60]. In addition, for the polymer/clay dispersions having the same clay loading level, but different surfactant chemistry, the NA dispersion exhibits the longest relaxation time, experimental time to break and De number, followed by the NB dispersion and then the NC dispersion. We attribute this observation primarily to the difference in the extent of intercalation and/or exfoliation of these clays as well as to the interfacial strength resulting from the association of the reactive tethering groups with the PMMA matrix, in accordance with the results seen in the morphology analysis and shear rheology analyses for the as-polymerized nanocomposites.

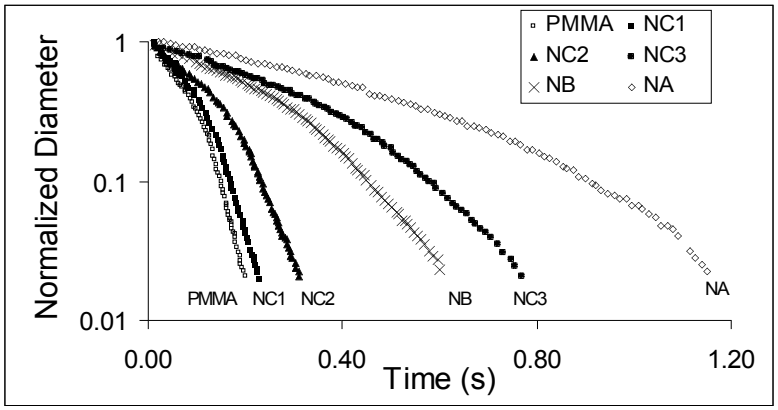

(a)

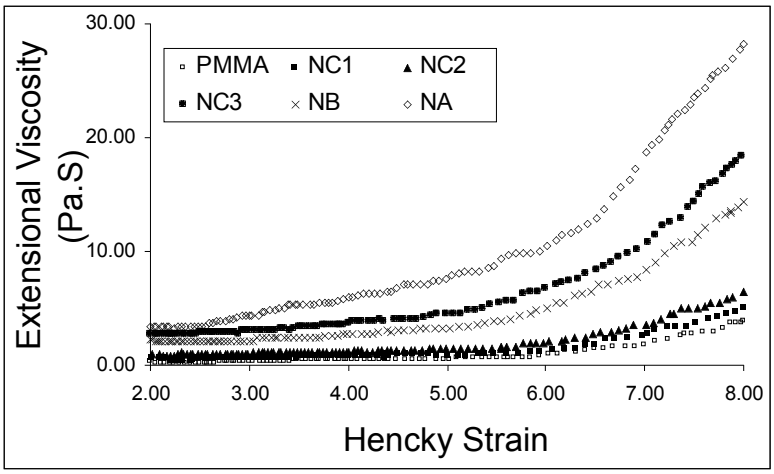

(b)

Figure 7. (a) Evolution of mid-filament diameter vs time and (b) apparent extensional viscosity vs Hencky strain for the 10 wt% PMMA solution and 10 wt.%PMMA/clay dispersions.

Table 2: Comparison of the longest relaxation time, λ_c, the experimental breaking time, t_b, and Deborah number, De, at different clay loading levels for the 10% PMMA solution and PMMA/clay dispersions.

	Clay loading (wt%)	λ_c (s)	t_b (s)	De
PMMA (10wt%)	0	0.0108	0.231	1.049
NA(10wt%)	2.5	0.0759	1.271	7.370
NB(10wt%)	2.5	0.0368	0.689	3.573
NC1(10wt%)	2.5	0.0126	0.265	1.223
NC2(10wt%)	5	0.0186	0.400	1.806
NC3(10wt%)	7.5	0.0473	0.908	4.592

Electrospinning:

The dependence of electrospinning upon different surfactant chemistry and clay loading levels was evaluated. In a previous paper, we demonstrated that extensional rheology combined with conductivity could be used to predict qualitatively the electrospinnability of polymer solutions and polymer/clay dispersions [29]. A longer relaxation time combined with higher conductivity indicates better electrospinnability of the fluids. It is noteworthy that the Hencky strain rate measured by CaBER is only in the range of 1-10 s^{-1}, while the extensional strain rate in the charged liquid jet during electrospinning is on the order of 10 s^{-1} in the steady jet regime [15], but could reach up to 100 s^{-1} at the whipping stage [60-66]. Therefore, the strain hardening measured by CaBER is another very important property indicator for prediction of electrospinnablity of polymer fluids. The conductivity of 10 wt.% PMMA solution and the PMMA/clay

dispersions are listed in Table 3. Addition of clay slightly increases the conductivity of polymer solution, possibly due to the ionic surfactants and polar nature of clays. The NA, NB and NC1 dispersions having the same loading level exhibit almost the same conductivity. For the NC dispersions, the conductivity increases slightly with respect to the clay loading. Based on these extensional rheology and conductivity data, we anticipate that the relative ease of electrospinning of PMMA solution and PMMA/clay dispersions should be as follow:

$$PMMA < NC1 < NC2 < NB < NC3 < NA$$

Table 3 lists the typical processing parameters used to electrospin the PMMA solutions and polymer/clay dispersions at concentrations of 6 wt.% and 10 wt.% by weight and the resulting fiber diameters. For the 6 wt.% solutions, a uniform fiber morphology is observed for the NA and NC3 dispersions, while a beads-on-string morphology is obtained for the PMMA solution and all of the other nanocomposite dispersions. At 5 wt%, the PMMA solution and all of the nanocomposite dispersions produce a beads-on-string morphology by electrospinning. These results are consistent with the prediction of electrospinnablity based on the extensional rheology and conductivity measurements. Therefore, we conclude that the NA dispersion has at least the same or better electrospinnablity than the NC3 dispersion, even though the latter has three times as much clay loading as the former. This indicates that it is the exfoliation of clay in combination with strong interphase strength, made possible by proper tethering chemistry, that improves the efficiency of clays in modifying solution properties and resulting fiber size. For the 10 wt.% solutions, uniform fibers were observed for all polymer solutions and polymer/clay dispersions, and the diameter of the electrospun

fibers are statistically the same. This indicates that, while incorporation of clays increases the electrospinnability of polymer solutions, the diameters of electrospun fibers are determined mostly by the total solids concentration, which consisted primarily of the polymer component. Due to the small amount of clay particles in the nanocomposites, the effect of clay particles on the diameter of the electrospun fibers are minimal. Therefore, one strategy to produce smaller diameter fibers is to electrospin more dilute polymer solutions that are rendered electrospinnable through the addition of well-exfoliated clay, which serves to impart increased extensional hardening to the fluid at low polymer concentrations. Figure 8 shows some representative SEM images of the electrospun fibers.

Table 3. Typical processing parameters used for electrospinning. Conductivity refers to the static conductivity of solution; voltage refers to the applied voltage; distance refers to the separation between nozzle and collection electrodes; current refers to that measured at the collector electrode [29, 51].

Polymer solutions or polymer/clay dispersions	Conductivity (μS/cm)	Voltage (kV)	Distance (cm)	Flow rate (ml/min)	Current (nA)	Fiber diameter (μm)
PMMA(6 wt.%)	7.26	14.5	40	0.015	38.5	Beads-on-string
NA (6 wt.%)	12.84	14.41	35	0.03	47.9	0.51±0.08
NB (6 wt.%)	9.37	14.1	35	0.03	45	Beads with fiber
NC1 (6 wt.%)	12.82	13.6	35	0.025	42	Beads-on-string
NC2 (6 wt.%)	17.78	13.4	35	0.02	42.5	Beads-on-string
NC3 (6 wt.%)	22.5	13.3	35	0.02	55.60	0.57±0.05
PMMA (10 wt.%)	8.31	12.4	35	0.02	35.4	1.60±0.36

NA (10 wt.%)	13.85	12.2	35	0.02	36.0	1.88±0.37
NB (10 wt.%)	15.19	13.4	35	0.01	29.5	1.72±0.22
NC1 (10 wt.%)	13.88	12.4	35	0.02	41.2	1.51±0.18
NC2 (10 wt%)	21.1	12.8	35	0.015	22.0	1.75±0.29
NC3 (10 wt%)	29.5	12.2	35	0.02	66.61	1.84±0.23

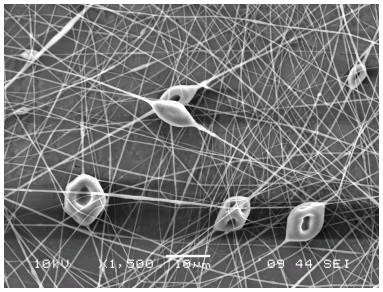

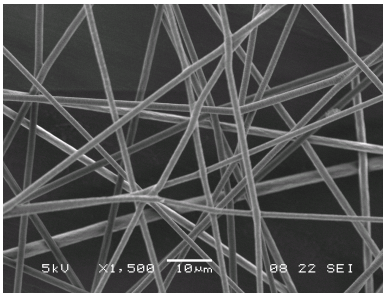

(a) (b)

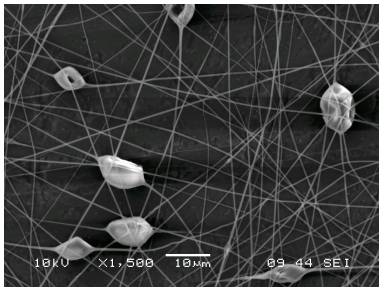

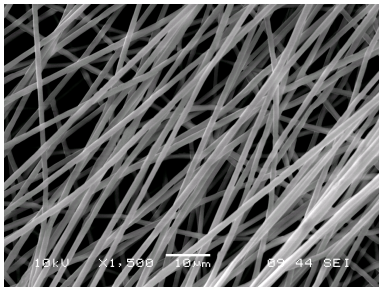

(c) (d)

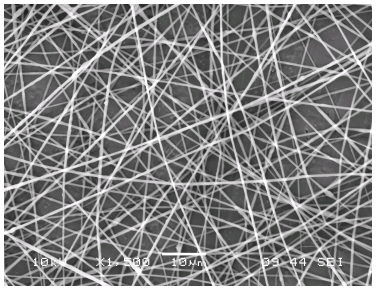

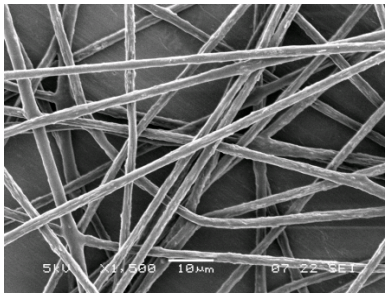

(e) (f)

Figure 8. Representative SEM images of electrospun fibers, (a) PMMA (6 wt.%), (b) PMMA (10 wt.%), (c) NC1 (6 wt.%), (d) NC1 (10 wt.%), (e) NA (6 wt.%), and (f) NA (10 wt.%). (All images have the same magnification, x1500).

In a previous paper**,** TEM images showed that MMT was well distributed within the electrospun fibers and oriented along the fiber axis direction. However, WAXD data for those nanocomposite fibers revealed a small peak associated with the basal reflection of MMT clays, indicative of incomplete exfoliation in the absence of any surfactant modification. [29]. In this study, the effect of surfactant chemistry on the exfoliation of clay within the electrospun fibers was also examined by WAXD. The WAXD spectra of electrospun fiber mats for pure PMMA, NC1 and NA are compared in Figure 9. NC1 fibers show a small peak at $2\theta = 3.50°$ with a corresponding d-spacing value of 2.5 nm, indicating the presence of intercalated morphology. However, no peaks are discernable for the NA fibers; the disappearance of WAXS signals could be due exfoliation or to extensive intercalation that shifts the diffraction peak below the detection limit in 2θ. These observations reveal that proper tethering chemistry is very important in improving the morphology of electrospun nanocomposite fibers. This improvement could be due to the improved intercalation and/or exfoliation of clays in the as-polymerized nanocomposites as well as the improved stability of the dispersions from which electrospun fibers are produced.

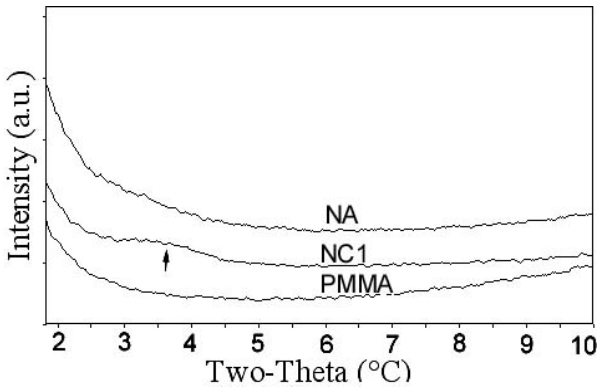

Figure 9: WAXD spectrums of electrospun PMMA fibers and PMMA/clay nanocomposite fibers.

Conclusions:

We examined the choice of tethering chemistry of cationic surfactants on exfoliation, electrospinnability and diameters of in-situ polymerized PMMA/montmorillonite (MMT) nanocomposite fibers by electrospinning. Incorporation of an additional reactive tethering group of methacryl functionality significantly improves the extent of intercalation/exfoliation of clays as well as the dispersion stability of in-situ polymerized PMMA nanocomposites. This was mainly attributed to the similarity of tethering chemistry to the MMA monomer and PMMA matrix as well as to the reaction of unsaturated vinyl groups with the MMA monomer. The shear and extensional viscosities of polymer/clay dispersions at low shear or extensional rates were increased by both increasing the loading level of clay particles and choosing the appropriate tethering chemistry of cationic surfactants. However, the proper surfactant chemistry is more effective in increasing the extensional viscosity than increasing the shear viscosity. The electrospinnability predicted based on both extensional rheology and conductivity measurements correlates well with electrospinning results from PMMA solution and

nanocomposite dispersions. Improved exfoliation of PMMA nanocomposites with methacryl-tethering clays leads to higher electrospinnability of these materials, a consequence of increased apparent extensional viscosity and strain hardening; the benefits of exfoliation equal or exceed those arising from addition of a three-fold higher loading of clay without any tethering groups.

Clays are predominately exfoliated in nanocomposite fibers containing methacryl-tethering clays, while the intercalated morphology is present in nanocomposite fibers containing commercial Cloisite™ 20A clay with no additional tethering group. The diameters of nanocomposite fibers were mostly determined by the total solids concentrations, which consist primarily of the polymer component. Due to the small amount of clay particles in the nanocomposite dispersions, the effect of clay particles on the diameter of the electrospun nanocomposite fibers is minimal. These observations clearly demonstrate a new strategy to produce smaller diameter of fibers from very dilute polymer solutions, which are otherwise not electrospinnable, by incorporating a small amount of well-exfoliated clays.

ACKNOWLEDGEMENTS

AJH thanks Triton Systems, Inc. for the PMMA nanocomposites which were synthesized and prepared under an Army Research Laboratory SBIR program, DAAD17-00-C-0091. Useful discussions with S.V. Fridrikh on extensional rheology and electrospinnability are gratefully acknowledged. This research was supported by the U.S. Army through the Institute for Soldier Nanotechnologies, under Contract DAAD-19-02-D0002 with the U.S. Army Research Office.

References:

1. Doshi J., Reneker DH J. Electrostat 1995; 35: 151-60.
2. Shin YM, Hohman MM, Brenner MP, Rutledge GC Polymer 2001; 42: 9955-67.
3. Tsai PP, Schreuder-Gibson H, Gibson P. J. Electrostat 2002; 54: 333-41.
4. Demir MM, Yilgor I, Yilgor E, Erman B. Polymer 2002; 43: 3303-9.
5. Ma ML, Hill RM, Lowery JL, Fridrikh SV, Rutledge GC Langmuir 2005; 21: 5549-54.
6. Wang M., Singh H., Hatton TA, Rutledge GC Polymer 2004; 45: 5505-14.
7. Wang M., Jin HJ, Kaplan DL, Rutledge GC Macromolecules 2004; 37: 6856-64.
8. Ko F. Gogotsi Y., Ali A., Naguib N., Ye H., Yang GL., Li C.,Willis P. Adv. Mater. 2003;15: 1161-5.
9. Bergshoef MM, Vancso GJ. Adv. Mater 1999; 11:1362-5.
10. Matthews JA., Wnek GE, Simpson DG Bowlin GL, Biomacromolecules 2002;3:232-8.
11. Reneker DH, Chun I. Nanotechnology 1996; 7: 216-23.
12. Yu JH, Fridrikh SV., Rutledge GC, Adv. Mater. 2004; 16: 1562-1566.
13. MacDiarmid AG, Jones WE, Norris ID, Gao J., Johnson AT, Pinto NJ, Hone J., Han B., Ko FK, Okuzaki H., Liaguno M., Synth Met, 2001;119:27-30.
14. Jin HJ, Fridrikh SV, Rutledge GC, Kaplan DL, biomacromolecules 2002;3:1233-1239.
15. Yu JH, Fridrikh SV, Rutledge GC, Polymer;2006; 47:4789-4797.

16. McKee MG, Wilkes GL, Colby RH, Long TE, Macromolecules 2004:,**37** 1760–1767

17. Gupta P., Elkins C., Long TE, Wilkes GL, Polymer 2005;46:4799-4810.

18. Shenoy SL, Bates WD, Frisch HL, Wnek GE, Polymer 2005; 46:3372-3384.

19. McKee MG, Layman JM, Cashion MP, Long TE, Science 2006;311:353-355.

20. Stefanescu EA, Petroven S., Daly WH, Negulescu II, Macromol. Mater. Eng., 2008;293;303-309.

21. Isci S., Unlu CH, Atici O., Gungor N., Bull. Mater. Sci.,2006; 29: 449–456.

22. Solar L., Nohales A., Espi RM, LoPez D., Gomez CM, Journal of Polymer Science: Part B: Polymer Physics,2008; 46: 1837–1844.

23. Cai YB 27 Li Q.27 Wei QF 27 Wu YB 27 Song L.27 Hu Y., J Mater Sci 2008; 43:6132–6138.

24. Ristolainen N.,Heikkila P., Harlin A.,Seppa J., Macromol. Mater. Eng. 2006; 291: 114–122.

25. Jeong KU, Chae HD, Lim C., Lee HK, Ahnc JH, Naha C.Polym Int 2010; 59: 249–255.

26. Park JH, Karim MR, Kim IK, Cheong IW, Kim JW, Bae DG, Cho JW,Yeum JH, Colloid Polym Sci 2010; 288:115–121..

27. Yu L., Cebe P., Polymer 2009; 50: 2133–2141.

28. Marras SI, Kladi KP , Tsivintzelis I., Zuburtikudis I., Panayiotou C., Acta Biomaterialia 2008; 4: 756–765.

29. Wang M., Hsieh AJ, Rutledge GC Polymer, 2005; 46: 3407-3418.

30. Ji Y., Li B., Ge S., Sokolove JC, Rafailovich MH, Langmuir, **2006**, 22 : 1321–1328

31. Park JH , Lee HW, Chae DK , Oh W., Yun JD , Deng Y. , Yeum JH, Colloid & Polymer Science 2009; 287:943-950.
32. Ji HM, Lee HW, Karim MR, Cheong IW, Bae EA, Kim TH, Islam MS, Ji BC, Yeum JH, Colloid Polym Sci 2009; 287:751–758
33. Karim MR, Lee HW, Kim R., Ji BC, Cho JW, Son TW, Oh W., Yeuma JH, Carbohydrate Polymers 2009; 78: 336–342
34. Marras SI, Kladi KP, Tsivintzelis I., Zuburtikudis I., Panayiotou C., Acta Biomaterialia 2008; 4: 756–765.
35. Neppalli R., Marega C. , Marigo A., Bajgai MP, Kim HY, Causin V., European Polymer Journal 2010; 46: 968–976.
36. Daga VK, Helgeson ME, Wagner NJ, Journal of Polymer Science: Part B: Polymer Physics, 2006; 44: 1608–1617.
37. Kojima Y., Usuki A., Kawasumi M., Okada A., Fukushima Y., Kurauchi T., J. Mater. Research 1993; 8:1185-89.
38. Messersmith P., Giannelis EP, Chem. Mater. 1993; 5: 1064-66.
39. Giannelis EP, Adv. Mater. 1996; 8: 29-35.
40. LeBaron PC, Wang, Z., Pinnavaia TJ, Appl. Clay Sci. 1999;15: 11-29.
41. Deitsche F., Thomann R., Thomann R., Mulhaupt , J. Apply. Polym. Sci. 2000; 75: 396-405.
42. Huang X., Brittain WJ, Macromolecules 2001;34: 3255-60.
43. Bandyopadhyay S., Hsieh AJ, Giannelis EP, ACS Symp. Series 2002; 804: 15-25.
44. Fan XW, Xia CJ, Advincula RC, Langmuir 2003; 19: 4381-89.
45. Fornes TD, Hunter DL, Paul DR, Macromolecules 2004; 37: 1793-1798.

46. Okamoto K., Ray SS, Okamoto M., Journal of polymer science, part B, 2003; 41: 3160-3172.

47. Yoon PJ, Hunter DL, Paul DR, Polymer 2003; 44: 5323-5339.

48. Kurian M., Dasgupta A., Beyer FL, Galvin ME, Journal of polymer science, polymer physics 2004; 42: 4075-4083.

49. Vaia R., Giannelis EP, Macromolecules 1997;30:7990-99.

50. Balazs AC, Singh C., Zhulina E., Macromolecules 1998;31:8370-81.

51. Fridrikh SV, Yu JH, Brenner MP, Rutledge GC, Phys. Rev. Lett. 2003; 90: 144502.

52. Shin M., Hohman MM, Brenner MP, Rutledge GC, Apply. Polym. Lett. 2001; 78: 1149-51

53. Zeng CC, Lee LJ, Macromolecules 2001; 34: 4098-4103.

54. Meneghetti P., Qutubuddin S., Langmuir 2004; 20; 3424-3430.

55. Hyun YH, Lim ST, Choi HJ, Jhon MS, Macromolecules 2001; 34: 8084-8093.

56. Krishamoorti R., Giannelis EP, Macromolecules 1997; 30; 4097-4102.

57. Schmidt G., Nakatani AI, Butler PD, Karim A., Han CC Macromolecules 2000; 33: 7219-7222.

58. Chen L., Bromberg L., Hatton TA, Rutledge GC, Polymer, 2008; 49:1266-1275.

59. Tanoue S., Utracki L., Garcia-Rejon A., Sammut P., Ton-That M., Pesneau I., Polym. Eng. Sci. 2004; 44: 1061-76.

60. Prasad R., Pasanovic-Zujo V., Gupta R., Cser F., Bhattacharya S., Polym. Eng. Sci. 2004; 44: 1220-30.

61. Hohman MM, Shin M., Rutledge GC, Brenner MP, Physics of Fluids 2001; 13:2201-2220.

62. Hohman MM, Shin M., Rutledge GC, Brenner MP, Physics of Fluids 2001; 13: 2221-2236.

63. Reneker DH, Yarin AL, Fong H., Koombhongse S., Journal of Applied Physics 2000; 87: 4531-4547.

64. Feng JJ, Physics of Fluids, 2002; 14: 3912-3926.

65. Yarin L., Koombhongse S., Reneker DH, Journal of Applied Physics 2001; 90: 4836-4846.

66. Fong H, Liu W., Wang CS, Vaia RA, Polymer 2002; 43: 775-80.

Figure 1: Alkyl ammonium surfactants with tethering group of either (a) methacryl or (b) styryl functionality.

Figure 2: Comparison of WAXD spectra of in-situ polymerized PMMA nanocomposites consisting of the same 2.5 wt.% MMT clays: NA, NB, NC1 .

Figure 3: Comparison of TEM images of in-situ polymerized PMMA nanocomposites consisting of the same 2.5 wt.% MMT clays (a), NA, (b), NB, (c), NC1.

Figure 4: The appearance of 6 wt% PMMAclay dispersions in DMF after storage for two weeks.

Figure 5. Steady shear viscosity as a function of shear rate measured at room temperature for 10 wt.% PMMA solution and 10 wt.% PMMA/clay dispersions.

Figure 6. Dynamic shear rheology data as a function of frequency for 10 wt% PMMA solution and 10 wt% PMMA/clay dispersions: (a) storage modulus, G', and (b) loss modulus, G".

Figure 7. (a) Evolution of mid-filament diameter vs time and (b) apparent extensional viscosity vs Hencky strain for the PMMA solution and 10 wt% PMMA/clay dispersions.

Figure 8. Representative SEM images of electrospun fibers, (a) PMMA (6 wt.%), (b) PMMA (10 wt.%), (c) NC1 (6 wt.%), (d) NC1 (10 wt.%), (e) NA (6 wt.%), and (f) NA (10 wt.%). (All images have the same magnification, x1500).

Figure 9: WAXD spectrums of electrospun PMMA fibers and PMMA/clay nanocomposite fibers.